

A unique mode of keratinocyte death requires intracellular acidification

Takeshi Matsui^{a,b,1,2}, Nanako Kadono-Maekubo^a, Yoshiro Suzuki^{c,3}, Yuki Furuichi^{a,b}, Keiichiro Shiraga^{a,4}, Hiroyuki Sasaki^a, Azusa Ishida^{d,e}, Sonoko Takahashi^{d,e}, Takaharu Okada^{d,e}, Kiminori Toyooka^f, Jafar Sharif^g, Takaya Abe^h, Hiroshi Kiyonari^h, Makoto Tominaga^c, Atsushi Miyawakiⁱ, and Masayuki Amagai^{a,b,1}

^aLaboratory for Skin Homeostasis, RIKEN Center for Integrative Medical Sciences, Yokohama 230-0045, Japan; ^bDepartment of Dermatology, Keio University School of Medicine, Tokyo 160-8582, Japan; ^cDivision of Cell Signaling, National Institute for Physiological Sciences, National Institutes of Natural Sciences, Okazaki 444-8787, Japan; ^dLaboratory for Tissue Dynamics, RIKEN Center for Integrative Medical Sciences, Yokohama 230-0045, Japan; ^eGraduate School of Medical Life Science, Yokohama City University, Yokohama, Kanagawa, 230-0045, Japan; ^fMass Spectrometry and Microscopy Unit, RIKEN Center for Sustainable Resource Science, Yokohama 230-0045, Japan; ^gLaboratory for Developmental Biology, RIKEN Center for Integrative Medical Sciences, Yokohama 230-0045, Japan; ^hLaboratory for Animal Resources and Genetic Engineering, RIKEN Center for Biosystems Dynamics Research, Kobe 650-0047, Japan; and ⁱLaboratory for Cell Function Dynamics, RIKEN Center for Brain Science, Wako 351-0198, Japan

Edited by Janet Rossant, The Gairdner Foundation, Toronto, ON, Canada, and approved March 8, 2021 (received for review November 7, 2020)

The stratum corneum (SC), the outermost epidermal layer, consists of nonviable anuclear keratinocytes, called corneocytes, which function as a protective barrier. The exact modes of cell death executed by keratinocytes of the upper stratum granulosum (SG1 cells) remain largely unknown. Here, using intravital imaging combined with intracellular Ca^{2+} - and pH-responsive fluorescent probes, we aimed to dissect the SG1 death process *in vivo*. We found that SG1 cell death was preceded by prolonged (~60 min) Ca^{2+} elevation and rapid induction of intracellular acidification. Once such intracellular ionic changes were initiated, they became sustained, irreversibly committing the SG1 cells to corneocyte conversion. Time-lapse imaging of isolated murine SG1 cells revealed that intracellular acidification was essential for the degradation of keratohyalin granules and nuclear DNA, phenomena specific to SC corneocyte formation. Furthermore, intravital imaging showed that the number of SG1 cells exhibiting Ca^{2+} elevation and the timing of intracellular acidification were both tightly regulated by the transient receptor potential cation channel V3. The functional activity of this protein was confirmed in isolated SG1 cells using whole-cell patch-clamp analysis. These findings provide a theoretical framework for improved understanding of the unique molecular mechanisms underlying keratinocyte-specific death mode, namely corneoptosis.

corneoptosis | cornification | cell death | acidification | keratinocytes

Cell death is an essential physiological phenomenon for the development and homeostasis of tissues and organs (1). To date, various types of cell death are classified according to their molecular and morphological features, including intrinsic/extrinsic apoptosis, mitochondrial permeability transition-driven necrosis, necroptosis, ferroptosis, pyroptosis, parthanatos, entotic cell death, NETotic cell death (NET: neutrophil extracellular traps), lysosome-dependent cell death, autophagy-dependent cell death, and immunogenic cell death (2). In these cell death types, the remnants of dead cells are removed by macrophages or adjacent cells through phagocytosis via efferocytosis. When dysregulated, the leakage of cellular contents, mitochondria, and DNA from dead cells can cause tissue inflammation (3). Notably, cell death generally implies the end of its functionality; dead cells and their products are generally unnecessary for organisms. However, in the case of epidermal keratinocytes, cell death does not indicate the end of their role; rather, dead epidermal keratinocytes converted into corneocytes constitute the stratum corneum (SC) that function as barriers (4–6). The SC enables terrestrial vertebrates to survive in the context of nonaquatic environments and even resist extreme environments by protecting the body against mechanical stresses, pathogen invasion, toxic substances, and dehydration (7).

Keratinocytes stem from the proliferative stratum basale (SB), differentiate, and move upward to form several stratum spinosum

layers (8) (Fig. 1A). Subsequently, they form three layers of the stratum granulosum (SG) (SG1–3, the more superficial to the deepest layer) with a flattened Kelvin's tetrakaidecahedron cell shape (9). Tight junctions (TJs), which enable individual cells to join as united topological barriers, are formed within the SG2 cell layer (10–12). SG1 cells above the TJs undergo cell death, forming a functional air–liquid interface barrier (i.e., the SC).

In dying SG1 cells, intracellular changes enable the generation of functional barrier materials. Unique biochemical reactions occur in dying SG1 cells, including 1) the exclusion of lamellar lipids from specialized secretory vesicles formed in the epidermis called lamellar granules to the extracellular space; 2) the cell membrane transition to cornified envelopes (CEs), with highly

Significance

In specific tissues, cell death does not represent the end of cell function. The death of the uppermost stratum granulosum keratinocytes (SG1 cells) facilitates their conversion into stratum corneum (SC) corneocytes. Such cells are not removed by efferocytosis as would occur after apoptosis or necrosis; instead, nonviable cell bodies contribute to the protective barrier function of the SC. The present study demonstrates that SG1 cell death is initiated via a single episode of prolonged intracellular Ca^{2+} elevation, followed by rapid acidification. Such intracellular ionic changes facilitate organellar degradation events specific to SC corneocyte formation. These findings further expand the current knowledge on cell death modes and highlight that nonviable cells contribute to physiological functions in specific contexts.

Author contributions: T.M., Y.S., T.O., M.T., and M.A. designed research; T.M., N.K.-M., Y.S., Y.F., H.S., A.I., and S.T. performed research; T.M., N.K.-M., Y.S., Y.F., K.S., T.O., K.T., J.S., T.A., H.K., and A.M. contributed new reagents/analytic tools; T.M., N.K.-M., Y.S., K.S., A.I., S.T., T.O., K.T., J.S., M.T., and A.M. analyzed data; and T.M. and M.A. wrote the paper.

The authors declare no competing interest.

This article is a PNAS Direct Submission.

Published under the PNAS license.

See [online](#) for related content such as Commentaries.

¹To whom correspondence may be addressed. Email: takeshi.matsui@riken.jp or amagai@keio.jp.

²Present address: School of Bioscience and Biotechnology, Tokyo University of Technology, Tokyo, 192-0982, Japan.

³Present address: Department of Physiology, Iwate Medical University, Iwate 028-3964, Japan.

⁴Present address: Division of Environmental Science and Technology, Graduate School of Agriculture, Kyoto University, Kyoto 606-8502, Japan.

This article contains supporting information online at <https://www.pnas.org/lookup/suppl/doi:10.1073/pnas.2020722118/-DCSupplemental>.

Published April 23, 2021.

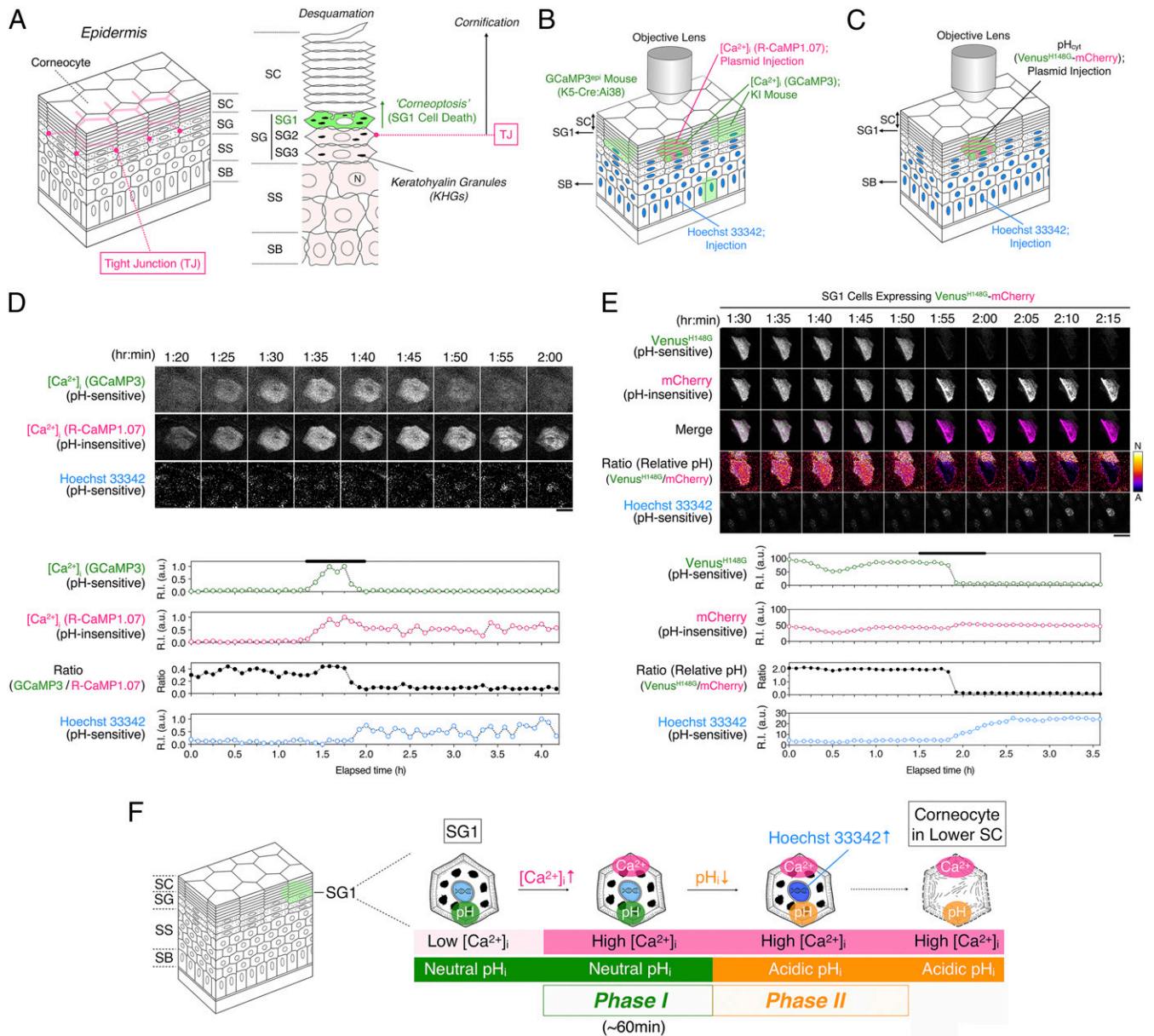


Fig. 1. Intracellular acidification of SG1 cells in vivo. (A) Structure of the epidermis. The epidermis is composed of the SB, stratum spinosum (SS), SG, and SC. The SG is composed of SG1 (green), SG2, and SG3 cell layers. TJs are formed between adjacent SG2 cells (magenta line). Cornification involves multiple processes, including cell death of SG1 cells to form corneocytes and maturation of corneocytes that will constitute the SC. Corneocytes eventually shed from the surface of the SC (Desquamation). Here, we termed SG1 cell death as “corneoptosis.” (B) A schematic illustration of the intravital double [Ca²⁺]_i imaging of SG1 cells coexpressing GCaMP3 (green) and R-CaMP1.07 (magenta) from the dorsal skin epidermis of an adult GCaMP3^{epi} hairless mouse. Hoechst 33342 and pCMV-R-CaMP1.07 plasmid were intraepidermally and sequentially injected into the mouse’s dorsal skin. (C) A schematic illustration of intravital pH_i imaging of SG1 cells expressing pHVenus-mCherry. Hoechst 33342 and the pCMV-pHVenus-mCherry plasmid were intraepidermally and sequentially injected into the dorsal skin of the adult hairless mice. (D) Representative time-lapse fluorescence images of an SG1 cell simultaneously expressing GCaMP3 and R-CaMP1.07a. Time-lapse images were obtained at 5 min intervals for 4 h 10 min. GCaMP3 fluorescence intensity gradually increased and peaked at around 1 h 45 min and then suddenly decreased to basal levels. R-CaMP1.07 fluorescence intensity peaked in a similar manner, but its levels remained high (scale bar, 20 μm). Changes in the fluorescent intensities of GCaMP3, R-CaMP1.07, and Hoechst 33342 signals detected in an SG1 cell plotted against the elapsed time. The fluorescence intensity ratios corresponding to the relative pH ratio (GCaMP3 to R-CaMP1.07) is shown. Notably, nuclear Hoechst 33342 intensity gradually increased after a decrease in the fluorescence intensity of GCaMP3. The black line indicates the duration time shown in images. See also *SI Appendix, Fig. S2 A and B* and *Movie S2*. (E) Representative time-lapse fluorescence images of an SG1 cell expressing the pHVenus-mCherry fusion protein and Hoechst 33342 are shown. Time-lapse images were obtained at a 5 min interval for 215 min. Immediately after the decrease in “cytoplasmic” pHVenus fluorescence intensity, Hoechst 33342 intensity gradually increased. In contrast, “cytoplasmic” mCherry intensity rarely changed (scale bar, 20 μm). Changes in the fluorescence intensities of pHVenus and mCherry detected in an SG1 cell are plotted against the elapsed time. Relative pH (ratio of pHVenus to mCherry signal) and Hoechst 33342 signal intensity are shown. Notably, just after the immediate cytoplasmic acidification of the SG1 cell, the Hoechst 33342 signal in the nucleus began to increase gradually. The black line indicates the duration time shown in images. See also *Movie S3*. (F) A schematic illustration of the changes observed in SG1 cell death via intravital imaging. Live SG1 cells exhibited a low [Ca²⁺]_i and neutral pH_i. Unidentified signal(s) induced an increase in [Ca²⁺]_i under a neutral pH_i for ~60 min (phase I). Then, the pH_i of SG1 cells decreased at high [Ca²⁺]_i (phase II). Hoechst 33342 intensity began to increase in phase II. We assumed that these conditions were maintained in corneocytes in the lower SC where DNA, keratohyalin granules, and organelles are lost.

cross-linked hydrophobic proteins produced by the activity of transglutaminases (TGases); 3) the formation of dense keratin networks; and 4) the degradation of organelles including the nucleus with terminal deoxynucleotidyl transferase-mediated dUTP Nick End Labeling–negative nuclear DNA, mitochondria, and Golgi complex, resulting in the formation of “corneocytes” (5, 6, 13–15). These processes contribute to the formation of the functional barrier component of the SC via further maturation of the corneocytes (16–19). The term “cornification” refers to the entire process of SC formation. Although the initial step in cornification is SG1 cell death, the molecular mechanisms are, to date, unclear owing to the lack of appropriate *in vivo* and *in vitro* experimental systems (20, 21).

Here, we combined various fluorescent probes and generated a system to dissect cell death in SG1 cells *in vivo* and *in vitro*. We analyzed major cytoplasmic events via intravital imaging of fluorescently labeled protein probes expressed in SG1 cells. To examine the impact of ionic changes in SG1 cells, we isolated and cultured them under different Ca^{2+} and pH conditions. Finally, we performed a whole-cell patch-clamp analysis of SG1 cells to identify the molecule(s) responsible for their unique physiological properties.

Results

A Single Long-Lasting Elevation in the Intracellular Ca^{2+} Levels of SG1 Cells Was Observed *In Vivo*. To monitor time-dependent changes in intracellular Ca^{2+} ($[\text{Ca}^{2+}]_i$) in the epidermis during cornification *in vivo*, we generated a mouse expressing GCaMP3 in the epidermis (GCaMP3^{epi}). We performed intravital imaging of GCaMP3 mice considering different ear epidermal depths (SB and SG planes) using two-photon microscopic analysis (*SI Appendix, Fig. S1 and Movie S1*). To detect SG1 cells based on the depth of the epidermis, nuclei of keratinocytes were stained using Hoechst 33342. Time-lapse imaging with 5 min intervals for 6 h revealed that numerous SG1 cells showed transient, long-lasting signals of GCaMP3 and a sudden drop after ~60 min as reported (22). Some SB cells increasingly exhibited a transient, spike-like increase in GCaMP3 signal lasting less than 5 min. In addition, the nuclear fluorescence intensity of Hoechst 33342 in SG1 cells gradually intensified when the elevated GCaMP3 signal faded (*SI Appendix, Fig. S1 C and E*). This increase in the Hoechst 33342 signal was routinely used as the reference time point for the *in vivo* study of SG1 cells.

Intracellular Acidification Occurs in SG1 Cells *In Vivo*. The fluorescence intensity of GCaMP3 is dependent on the surrounding pH (23). R-CaMP1.07 is another fluorescent $[\text{Ca}^{2+}]_i$ indicator derived from red fluorescent protein; of note, its fluorescence is resistant to changes in the surrounding pH (24, 25). To test whether the observed reduced GCaMP3 signals were attributable to the intracellular acidification of SG1 cells *in vivo*, we devised a strategy that allowed the simultaneous expression of GCaMP3 and R-CaMP1.07 in single SG1 cells *in vivo*. We injected Hoechst 33342 intraepidermally, followed by a mammalian expression vector encoding R-CaMP1.07 into the dorsal skin of GCaMP3^{epi} hairless mice and subsequently proceeded to confocal microscopy (Fig. 1 *B and D, SI Appendix, Fig. S2 A and B, and Movie S2*). GCaMP3 signal in single SG1 cells was sustained for ~60 min and decreased subsequently. Importantly, the coexpressed R-CaMP1.07 signal intensity also gradually increased similarly to that of GCaMP3. However, the elevated signal of this pH-insensitive reporter was sustained (Fig. 1*D* and *SI Appendix, Fig. S2B*). The fluorescent ratio values of GCaMP3 to R-CaMP1.07 plotted against the elapsed time revealed that the simultaneous elevation of GCaMP3 and R-CaMP1.07 was followed by the reduction in GCaMP3 signals within 5 min. These results suggest that after a long-lasting $[\text{Ca}^{2+}]_i$ elevation at a neutral pH in the SG1 cells, rapid intracellular acidification

may occur while $[\text{Ca}^{2+}]_i$ remains elevated. Importantly, we confirmed that Hoechst 33342 signals were gradually increased even after GCaMP3 signals decreased in all SG1 cells (Fig. 1*D, SI Appendix, Fig. S2B, and Movie S2*).

To confirm that the decrease in the GCaMP3 signal in SG1 cells correlated with a drop in the cytoplasmic pH *in vivo*, we attempted to visualize the pH change in SG1 cells. First, we developed a ratiometric pH probe. To achieve pH ratiometric imaging, we fused the pH-sensitive and -insensitive pHVenus and mCherry proteins, respectively [pHVenus–mCherry; *SI Appendix, Fig. S2C* (26)]. As this fusion protein expresses pHVenus and mCherry at same molar ratio, we observed relative pH changes via simultaneous ratiometric imaging. To validate the ratiometric changes in fluorescence levels of pHVenus–mCherry, we expressed it in HeLa cells by transient transfection. Formalin-fixed HeLa cells were stained with Hoechst 33342 and treated with phosphate buffers (pH 7.23, pH 6.37, and pH 5.60). pHVenus–mCherry was expressed in the cytoplasm and nucleus of HeLa cells (*SI Appendix, Fig. S2D*). The fluorescence of pHVenus was decreased at lower pH, whereas that of mCherry remained unaltered. Of note, Hoechst 33342 signals were increased at lower pH, suggesting that the fluorescence intensity of Hoechst 33342 in chemically fixed HeLa cells is affected by the pH. To observe the changes in intracellular pH (pH_i) in SG1 cells *in vivo*, we intraepidermally injected Hoechst 33342 and the pCMV–pHVenus–mCherry plasmid into the dorsal skin of hairless mice (*SI Appendix, Fig. S3 and Movie S3*). Time-lapse confocal microscopic imaging revealed that SG1 cells expressing pHVenus–mCherry showed a time-dependent decrease in pHVenus fluorescence intensity, whereas that of mCherry rarely changed (Fig. 1 *C and E and Movie S3*). We speculate that living SG1 cells have a neutral pH_i , and acidification occurs when pHVenus fluorescence decays. Of note, Hoechst 33342 signal was inversely related to that of pHVenus, indicating that this acidification of SG1 cells occurred after a long-lasting $[\text{Ca}^{2+}]_i$ elevation.

Two High $[\text{Ca}^{2+}]_i$ Phases Are Observed in Dying SG1 Cells *In Vivo*.

Intravital imaging of SG1 cells *in vivo* revealed that SG1 cells go through two phases during cell death (Fig. 1*F*). In phase I, SG1 cells exhibited high $[\text{Ca}^{2+}]_i$ and neutral pH_i for ~60 min (phase I; high $[\text{Ca}^{2+}]_i$ -neutral pH_i). Then, in phase II, pH_i dropped rapidly while high $[\text{Ca}^{2+}]_i$ was sustained (phase II; high $[\text{Ca}^{2+}]_i$ -acidic pH_i). Having defined the characteristic phases of SG1 cell death *in vivo*, we next used primary cultured SG1 cells to study *in vitro* the mechanisms by which program(s) that coordinate these changes are maintained and controlled.

Isolation of Intact SG1 Cells from Mouse Skin. The primary culture of SG1 cells requires specific isolation of these cells with high purity. To achieve this, we generated knock-in mice expressing enhanced green fluorescent protein (EGFP) in the SG1 cell layer of the epidermis (EGFP^{SG1} mice; *SI Appendix, Fig. S4 A–E*). Intraepidermal injection of recombinant exfoliative toxin-A (ETA) protein into the dorsal skin of EGFP^{SG1} hairless mice resulted in the separation of the upper epidermal sheet containing the SG1, SG2, and SC layers (*SI Appendix, Fig. S4 F and G*) (20, 27). Subsequent trypsin treatment resulted in the isolation of SG1/2 cells (*SI Appendix, Fig. S4H*). Phase-contrast imaging revealed that SG1 (EGFP-positive) and SG2 (EGFP-negative) cells are morphologically indistinguishable from each other and contain numerous keratohyalin granules (KHGs) (Fig. 2*A*). Confocal microscopy analysis of isolated SG1 cells revealed that they maintained a polygonal saucer-like morphology (Fig. 2*B* and *Movie S4*). Scanning electron microscopic analysis of SG1 cells revealed that SG1 cells were shaped as Kelvin’s tetrakaidcahedron [Fig. 2 *C and D* (9)]. Moreover, their cell surface was covered with numerous fungiform protrusions and microvilli (Fig. 2*C*).

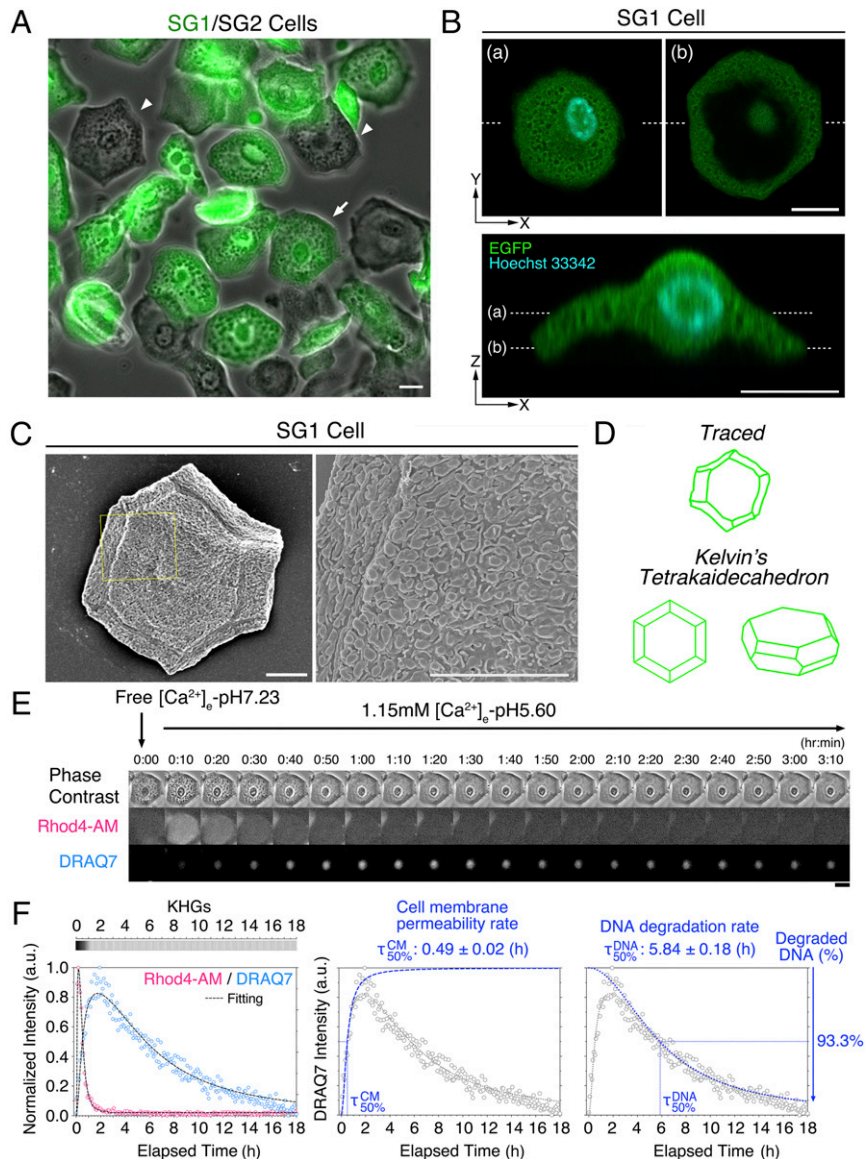


Fig. 2. Isolation of mouse SG1 cells and identification of the cornification-triggering agent. (A) Isolated SG1 (EGFP-positive; green) and SG2 (EGFP-negative) cells obtained from ETA sheets of adult hairless EGFP^{SG1} mice. The arrow indicates the SG1 cell analyzed in E–F. The arrowheads indicate EGFP-negative SG2 cells (scale bars, 20 μm). (B) Confocal microscopic X–Y- and Z-sectioning image of an isolated SG1 cell (EGFP; green) stained with Hoechst 33342 (cyan). Plane (a) and (b) of the X–Y-scanning image were indicated by dashed lines (scale bars, 10 μm). See also [Movie S4](#). (C) Scanning electron microscopic image of isolated SG1 cells. The yellow boxed areas are enlarged (*Right*). SG1 cells were covered with numerous fungiform protrusions and short microvilli (scale bars, 10 μm). (D) Traced images of E (*Upper illustration*) showed that isolated SG1 cell shape is similar to Kelvin’s tetrakaidecahedron (*Lower illustration*). (E) Representative time-lapse images of SG1 cells treated with high $[\text{Ca}^{2+}]_i$ -pH5.60 were captured every 5 min for 18 h. The morphology of KHGs was observed via phase-contrast microscopy. Rhod4-AM intensity was determined to measure relative $[\text{Ca}^{2+}]_i$. Cell membrane permeability was monitored via DRAQ7 nuclear staining. Rhod4-AM signals were highly and immediately increased at 10 min, followed by a gradual decrease within 1 h. Cell membrane permeability reached the maximum around 2 h after $[\text{Ca}^{2+}]_i$ increase, followed by a gradual decrease up to 18 h. KHGs were rapidly eliminated within 1 h (scale bar, 20 μm). See also [Movie S5](#). (F) Fluorescence intensity plots of Rhod4-AM and DRAQ7 against the elapsed time (18 h) (*Left*). The dashed lines indicate the fitting curves that reproduce experimental Rhod4-AM (magenta open circles) and DRAQ7 (blue open circles) signals. Time-dependent morphological changes in KHGs from 0 to 18 h are shown in the gray-scaled heatmap (whose depth of color depicts the presence of KHGs). Decomposed sigmoidal functions of 1) cell membrane permeability (*Middle*) and 2) DNA degradation (*Right*) compared with the experimental fluorescence intensity (open gray circles) and the best-fitted curve (blue dotted lines) for DRAQ7. The cell membrane permeability rate ($\tau_{50\%}^{\text{CM}}$) and the DNA degradation rate ($\tau_{50\%}^{\text{DNA}}$) were defined as the time required to obtain half of the final values for each sigmoidal curve, respectively.

High Ca^{2+} and Low pH Levels Induce Morphological Changes in Isolated SG1 Cells In Vitro. To reconstitute the intracellular changes in SG1 cells observed in vivo, we cultured SG1 cells in the context of different Ca^{2+} levels and pH levels. To assess both cell viability and the degradation of nuclear DNA, we used DRAQ7. An increase in the intensity of nuclear DRAQ7 corresponds to an increase in cell membrane permeability. To

monitor $[\text{Ca}^{2+}]_i$, we used the fluorescent Ca^{2+} indicator, Rhod4-AM. The morphology of KHGs of SG1 cells was observed via phase-contrast microscopy.

High $[\text{Ca}^{2+}]_i$ and low pH_i , as phase II conditions, were observed in the intravital imaging of SG1 cells in vivo (Fig. 1). To examine conditions under which isolated SG1 cells undergo changes consistent with those observed in vivo, we cultured

isolated SG1 cells under high $[Ca^{2+}]_e$ (1 mM) levels at an acidic pH_e (pH 5.60) (“high $[Ca^{2+}]_e$ -pH_e5.60”; Fig. 2 E and F and Movie S5). First, SG1 cells were suspended in “free $[Ca^{2+}]_e$ -pH_e7.26”

conditions. After the medium was changed to “high $[Ca^{2+}]_e$ -pH_e5.60,” the Rhod4-AM intensity in most SG1 cells increased at 5 to 10 min, followed by a rapid decrease within 1 h, owing to the

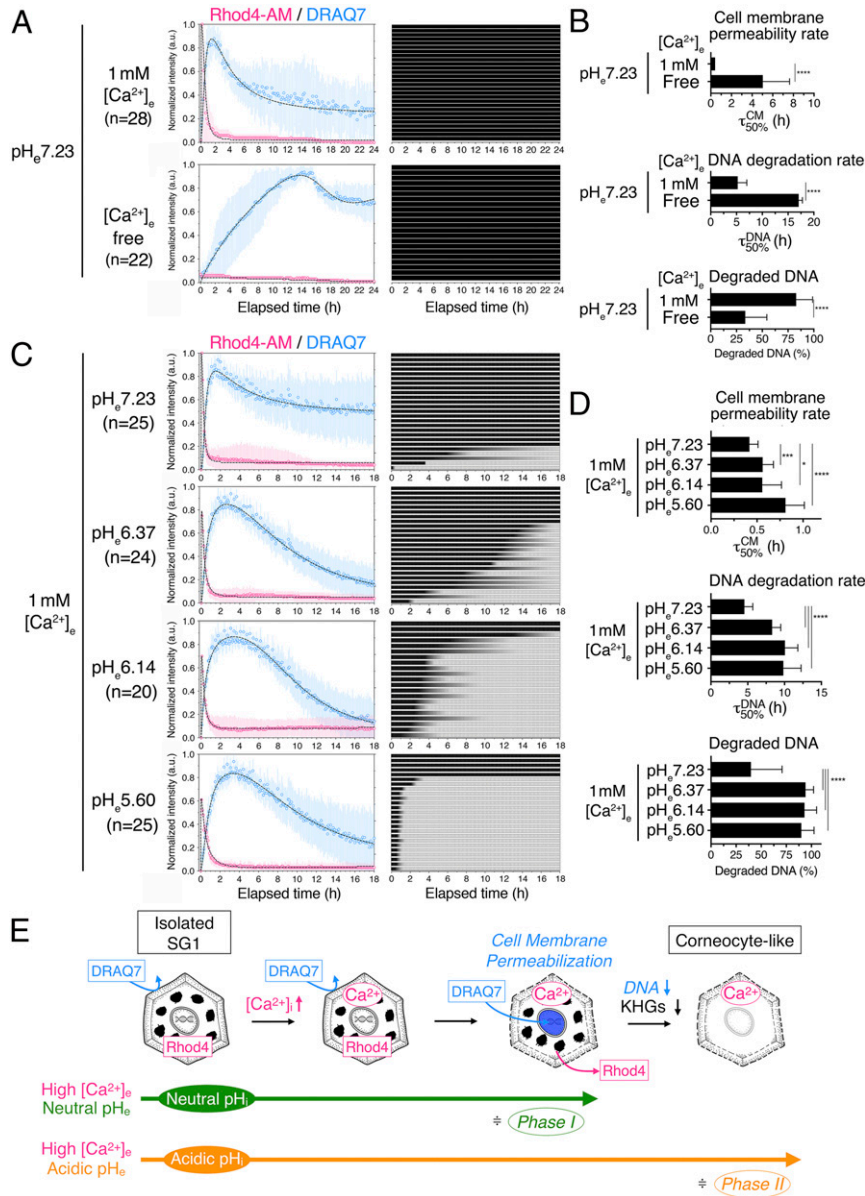


Fig. 3. High $[Ca^{2+}]_e$ and acidic pH_e values differentially induce corneocyte-related morphological changes in isolated SG1 cells in vitro. (A) Time-dependent changes in the fluorescence intensities of Rhod4-AM and DRAQ7 in SG1 cells treated with 1 mM ($n = 28$) or free ($n = 22$) $[Ca^{2+}]_e$ under neutral pH_e conditions (Left). The best-fit curves with the experimental intensity plot are shown by dashed lines. High $[Ca^{2+}]_e$ caused an increase in $[Ca^{2+}]_i$, followed by cell membrane permeabilization within 2 h. The gradual degradation of nuclear DNA was not completed. In contrast, free $[Ca^{2+}]_e$ hardly induced elevations in $[Ca^{2+}]_i$ and cell membrane permeabilization. Each row of the heatmap depicts the time-dependent changes of the presence of KHGs (black color corresponds to an unchanged quantity of KHGs). (B) The cell membrane permeability rate ($\tau_{50\%}^{CM}$) and DNA degradation rate ($\tau_{50\%}^{DNA}$) derived from the dual-sigmoidal curve fitting of DRAQ7 intensity in A. The uncertainty corresponds to the SD of the derived $\tau_{50\%}$. **** $P < 0.0001$. See also *SI Appendix, Table S1*. (C) Time-dependent changes in the fluorescence intensities of Rhod4-AM and DRAQ7 in isolated SG1 cells treated with different pH_e (7.23 ($n = 25$), 6.37 ($n = 24$), 6.14 ($n = 20$), and 5.60 ($n = 25$)) at 1 mM $[Ca^{2+}]_e$ (Left). Irrespective of pH_e , $[Ca^{2+}]_i$ elevation was induced, followed by cell membrane permeabilization within 2 to 3 h. Only under the highest pH_e (pH 7.23), an incomplete gradual decrease in DRAQ7 intensity was observed. The time-dependent changes in the presence of KHGs (darker color corresponds to a greater quantity of KHGs) showed that the dissipation rate of KHGs increased with decreasing pH_e (Right heatmap). (D) The $\tau_{50\%}^{CM}$ and $\tau_{50\%}^{DNA}$ with their SDs given in C are shown (Right). * $P < 0.05$, *** $P < 0.0005$, and **** $P < 0.0001$. See also *SI Appendix, Table S1*. (E) Schematic representation of the morphological changes observed in isolated SG1 cells in vitro. When SG1 cells preincubated with Rhod4-AM (Rhod4) were treated with “high $[Ca^{2+}]_e$ -neutral pH_e ” (phase I-mimicking conditions) in the presence of extracellular DRAQ7, an increase in $[Ca^{2+}]_i$ was induced, as shown by the increase in cytoplasmic Rhod4 signals. Then, cell membrane permeabilization occurred, and extracellular DRAQ7 was incorporated into the nucleus and intercalated to nuclear DNA, while Rhod4 simultaneously leaked out. This “high $[Ca^{2+}]_e$ -neutral pH_e ” is not sufficient to cause further intracellular changes in SG1 cells. In contrast, “high $[Ca^{2+}]_e$ -acidic pH_e ” (phase II-mimicking conditions) induced additional DNA degradation and KHG elimination after the increase in $[Ca^{2+}]_i$ and cell membrane permeabilization.

diffusion of Rhod4-AM along with increased cell membrane permeability. Additionally, the DRAQ7 intensity gradually increased for up to 2 h. Importantly, nuclei shrank, and nuclear DRAQ7 signals also decreased gradually for up to 18 h, suggesting that DNA degradation had occurred. KHGs gradually disappeared within 90 min resulting in a corneocyte-like appearance.

We sought to derive numerical values to summarize (and quantify) the temporal changes we observed in individual SG1

cells. To this end, we fit Rhod4-AM and DRAQ7 fluorescence intensities into sigmoidal functions (*SI Appendix, Eq. S1*), which were consistently well matched to the experimental results (Fig. 2*F*). Therefore, we used the intensity *I* and the 50% transition time $\tau_{50\%}$ values given by these modeled functions to quantify the characteristic temporal patterns of fluorescence from SG1 cells in various conditions. With regards to DRAQ7, we particularly termed $\tau_{50\%}^1$ and $\tau_{50\%}^2$ as “cell membrane permeability rate” ($\tau_{50\%}^{CM}$)

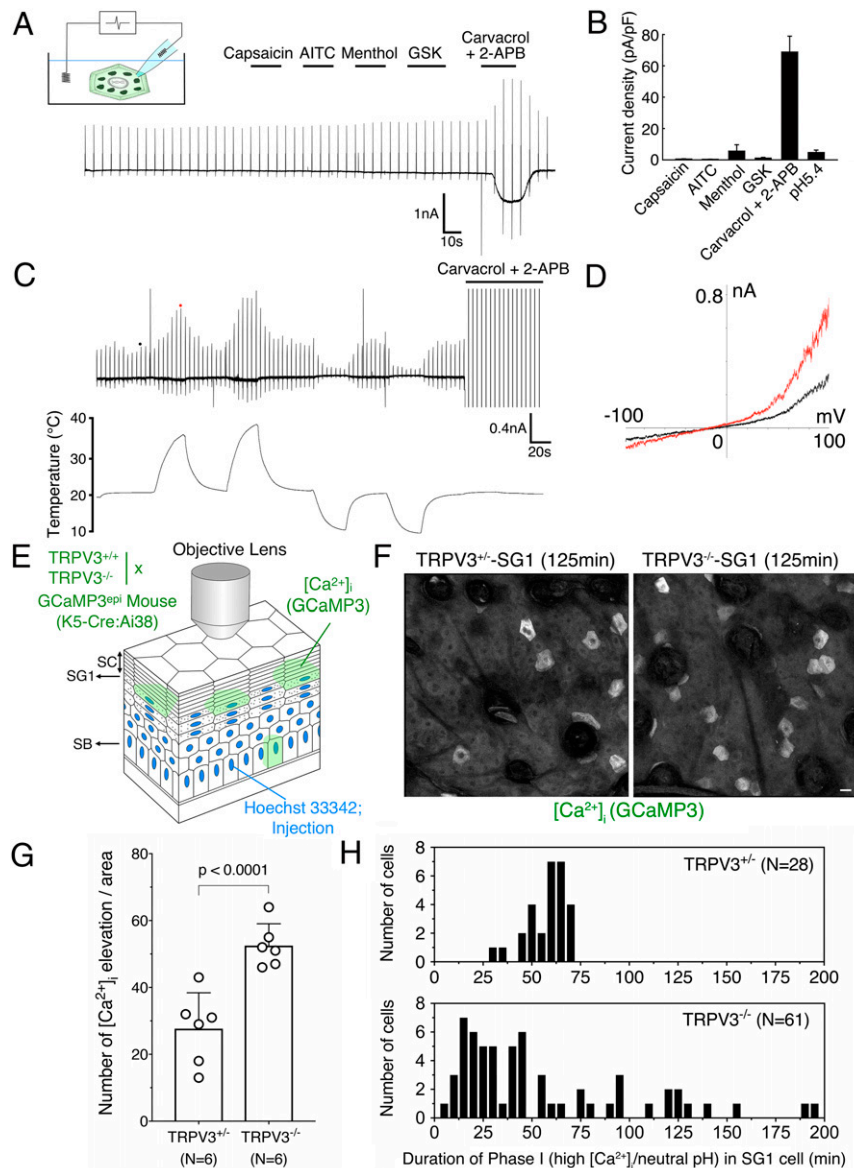


Fig. 4. TRPV3 regulates the $[Ca^{2+}]_i$ elevation and intracellular acidification timing occurred in SG1 cells. (A) A representative membrane current trace from whole-cell patch-clamp recordings in isolated SG1 cells is shown. Large currents were observed upon stimulation with TRPV3 activators (250 μ M carvacrol and 100 μ M 2-APB) but not with TRPV1 (1 μ M capsaicin), TRPA1 (100 μ M AITC), TRPM8 (100 μ M menthol), or TRPV4 agonists (0.5 μ M GSK1016790A) ($n = 6$). (B) The peak current density was increased by TRPV3 channel activators ($n = 4$ to 6) and not by a pH 5.4 ($n = 2$). (C) A representative membrane current trace of changes in temperature in isolated SG1 cells. Large currents were observed upon warm stimulation ($n = 4$). After two rounds of warm stimulation, an SG1 cell was stimulated with 250 μ M carvacrol and 100 μ M 2-APB (The peak current was out of range because the current was too large). (D) Current–voltage relationship of warm temperature–evoked currents is shown in the *Right* graph. The black and red dots in trace C indicate points where current–voltage curves were generated. (E) A schematic illustration of intravital GCaMP3 imaging in TRPV3^{-/-} mice. Time-lapse images of GCaMP3 and Hoechst 33342 were obtained at 5 min intervals for 305 min. The scanned plane containing SG1 cells is indicated by an arrow. (F) Representative images of TRPV3^{+/+} and TRPV3^{-/-} SG1 cells obtained from GCaMP3^{epi} mice at the 125 min time point of intravital imaging. Notably, the number of SG1 cells exhibiting increased GCaMP3 signals were increased in TRPV3^{-/-} SG1 cells (scale bar, 20 μ m). See also *SI Appendix, Fig. S4* and *Movie S7*. (G) The number of cells exhibiting elevation in $[Ca^{2+}]_i$ is shown in the bar graph. Time-lapse images of five different areas of TRPV3^{+/+} ($n = 6$) or TRPV3^{-/-} ($n = 6$) epidermis were obtained via confocal microscopy and analyzed. The number of SG1 cells exhibiting increased $[Ca^{2+}]_i$ was counted. TRPV3^{-/-} SG1 cells showed an increased elevation in $[Ca^{2+}]_i$. (H) The number of cells was plotted against the duration time of phase I (high $[Ca^{2+}]_i$ -neutral pH_i) for TRPV3^{+/+} ($n = 28$) or TRPV3^{-/-} ($n = 61$) SG1 cells.

and “DNA degradation rate” ($\tau_{50\%}^{\text{DNA}}$), which represents half of the time required to incorporate DRAQ7 into nuclear DNA and DNA degradation, respectively. We also defined the intensity of the declining sigmoidal component, I_{DNA} ($0 \leq I_{\text{DNA}} \leq 1$), as the ratio of “degraded DNA.” As shown in Fig. 2F, the best-fitted DRAQ7 intensity curve of a typical SG1 cell showed that $\tau_{50\%}^{\text{CM}}$ was 0.49 ± 0.02 h and $\tau_{50\%}^{\text{DNA}}$ was 5.84 ± 0.18 h, with the “degraded DNA” ratio of 100% (fully degraded DNA) in the “high $[\text{Ca}^{2+}]_e$ -pH5.60” condition. These indices enable us to quantitatively compare the intensity and rate of DRAQ7 signal changes.

Verification of the Effects of Phase I and II Conditions in Isolated SG1 Cells. Our intravital imaging revealed that cell death in SG1 cells proceeded in two phases, phase I (high $[\text{Ca}^{2+}]_i$ -neutral pH_i) and phase II (high $[\text{Ca}^{2+}]_i$ -acidic pH_i) (Fig. 1F). To address the biological significance of these two conditions, we cultured isolated SG1 cells and analyzed them under various $[\text{Ca}^{2+}]_e$ and pH_e conditions (Fig. 3).

Comparison of Changes in SG1 Cells Subjected to High- and Free- $[\text{Ca}^{2+}]_e$ Conditions at Neutral pH_e (Verification of Phase I Conditions). First, to address the effect of phase I conditions (high $[\text{Ca}^{2+}]_i$ -neutral pH_i) on SG1 cells, we examined the effect of high (1 mM) or free (0.21 nM) $[\text{Ca}^{2+}]_e$ on isolated SG1 cells under a neutral pH_e (pH 7.23) (Fig. 3A and B). Isolated SG1 cells were stimulated with either “high $[\text{Ca}^{2+}]_e$ -pH_e7.23” or “free $[\text{Ca}^{2+}]_e$ -pH_e7.23” media. In “high $[\text{Ca}^{2+}]_e$ -pH_e7.23,” SG1 cells showed an elevation in Rhod4-AM signals within 5 min, followed by a rapid decrease, possibly due to the permeabilized cell membrane. Consistently, DRAQ7 intensity was rapidly increased and maintained for up to 2 h, suggesting an increase in cell membrane permeability ($\tau_{50\%}^{\text{CM}}$; Fig. 3A and B and *SI Appendix, Table S1*). In contrast, under “free- $[\text{Ca}^{2+}]_e$ -pH_e7.23” conditions, Rhod4-AM signals increased to a lesser degree. DRAQ7 intensity rose slightly over 14 h, suggesting that cell membrane permeabilization occurred slowly ($\tau_{50\%}^{\text{CM}}$; Fig. 3A and B and *SI Appendix, Table S1*). Besides, the decrease of DRAQ7 intensity at the single-cell level indicated that partial DNA degradation was more frequent under “high- $[\text{Ca}^{2+}]_e$ -pH_e7.23” conditions than in the “free- $[\text{Ca}^{2+}]_e$ -pH_e7.23” ones ($\tau_{50\%}^{\text{DNA}}$; Fig. 3A and B and *SI Appendix, Table S1*). Both conditions revealed that most cells did not eliminate their KHGs (Fig. 3A (heat map) and Fig. 3E). As a result, degraded DNA (%) in “free- $[\text{Ca}^{2+}]_e$ -pH_e7.23” conditions was lower than that in “high- $[\text{Ca}^{2+}]_e$ -pH_e7.23” conditions (Fig. 3A, B, and E and *SI Appendix, Table S1*).

Comparison of Changes in SG1 Cells in High $[\text{Ca}^{2+}]_e$ in the Context of Various pH_e (Verification of Phase II Conditions). To examine the effect of phase II conditions (high $[\text{Ca}^{2+}]_i$ -acidic pH_i) on isolated SG1 cells, we tested four different pH_e conditions (pH 7.23, 6.37, 6.14, and 5.60) at high (1 mM) $[\text{Ca}^{2+}]_e$ (Fig. 3C and D and *Movie S6*). Under all pH_e conditions, isolated SG1 cells showed a similar increase in Rhod4-AM intensity immediately after the culture medium replacement, followed by cell membrane permeabilization. More specifically, the cell membrane permeability rate ($\tau_{50\%}^{\text{CM}}$) revealed that lower-pH conditions slowed the permeabilization of the SG1 cells ($\tau_{50\%}^{\text{CM}}$; Fig. 3C and D and *SI Appendix, Table S1*). The lower pH_e also retarded the rate of nuclear DNA degradation ($\tau_{50\%}^{\text{DNA}}$). However, the amount of degraded DNA increased under a lower pH_e. The most striking difference was in the elimination of KHGs. The number of cells exhibiting KHG elimination increased at a lower pH_e (Fig. 3C and E). Furthermore, the isolated SG1 cells were stimulated with “free- $[\text{Ca}^{2+}]_e$ -pH_e6.14” or “high- $[\text{Ca}^{2+}]_e$ -pH_e6.14” media. DNA and KHG degradation in SG1 cells decreased upon stimulation with “free- $[\text{Ca}^{2+}]_e$ -pH_e6.14” media compared to that observed

upon stimulation with “high- $[\text{Ca}^{2+}]_e$ -pH_e6.14” media (*SI Appendix, Fig. S5 and Table S1*), indicating that DNA degradation and KHG elimination require high $[\text{Ca}^{2+}]_e$.

Taken together, these results suggested that both high Ca^{2+} levels and acidic pH are required to degrade the DNA and KHGs.

Functional TRPV3 Is Highly Expressed in SG1 Cells. To further address how $[\text{Ca}^{2+}]_i$ and pH_i are regulated in SG1 cells, we investigated the Ca^{2+} influx-regulated membrane properties of SG1 cells. Epidermal and ETA sheets containing SG1/SG2 cells were isolated from adult C57BL6/N mice ear skin ($n = 3$). Their total RNAs were subjected to RNA-seq analysis. We first examined the expression of transient receptor potential (TRP) channels in SG cells as attractive candidates for molecules regulating $[\text{Ca}^{2+}]_i$ of SG1 cell. We analyzed the mRNA for all TRP channels, including TRPA, TRPC, TRPM, TRPP, and TRPV members. We found that *Trpm7*, *Trpp1*, and *Trpv6* were slightly expressed in SG1/2 cells and highly expressed in the epidermis (*SI Appendix, Fig. S6*). In contrast, *Trpm4*, *Trpm11*, *Trpv3*, and *Trpv4* were highly expressed in SG cells. To get a clear idea of the electrophysiological characteristics of SG1 cells, we used a whole-cell patch-clamp assay. We treated SG1 cells with TRP channel activators, including capsaicin (TRPV1), AITC (TRPA1), menthol (TRPM8), GSK1016790A (TRPV4), and carvacrol/2-APB (TRPV3) (Fig. 4A). The single SG1 cell recordings indicated that TRPV3 activators (carvacrol/2-APB) evoked large currents but capsaicin (TRPV1), AITC (TRPA1), menthol (TRPM8), and GSK1016790A (TRPV4) did not ($n = 6$). There was no obvious acid-sensing ion channel-like transient currents when an acidic solution (pH 5.4) was applied (Fig. 4B; $n = 2$). To determine whether the observed currents were derived from endogenous TRPV3, we modulated the bath temperature via the addition of preheated or cooled bath solutions after lifting the cell from the bottom of the recording chamber with the help of the patch pipette (Fig. 4C). Interestingly, we observed warm temperature-evoked currents, which is consistent with the previous reports that TRPV3 is activated at ambient temperature (32 to 39 °C) (28, 29) (Fig. 4C and D).

Alteration of the Frequency of $[\text{Ca}^{2+}]_i$ Elevation and the Intracellular Acidification Timing in TRPV3-Deficient SG1 Cells In Vivo. To test the physiological role of TRPV3 on SG1 cell death, we generated *Trpv3* knockout (TRPV3^{-/-}) hairless mice expressing GCaMP3 in the epidermis and subjected them to intravital $[\text{Ca}^{2+}]_i$ imaging (Fig. 4E). Three-dimensional time-lapse images of GCaMP3 fluorescence signals were obtained in the mouse back skin epidermis via confocal microscopy every 5 min for 305 min (Fig. 4F, *SI Appendix, Figs. S7 and S8*, and *Movie S7*). Z projection images of the epidermis revealed that TRPV3^{-/-}-SG1 had an increased frequency of $[\text{Ca}^{2+}]_i$ elevation per epidermal area, compared to that in heterozygous (TRPV3^{+/-}) mice (Fig. 4F and G and *SI Appendix, Figs. S7 and S8*). Strikingly, the duration time of sustained elevation of GCaMP3 signals was dysregulated and became either prolonged or shortened in TRPV3^{-/-}-SG1 cells (2~195 min), compared to that in TRPV3^{+/-}-SG1 cells (approximately ~60 min; Fig. 4H and *SI Appendix, Figs. S7B and S8*). The increase in Hoechst 33342 signals was detected after the drop of the elevated GCaMP3 signal in both TRPV3^{+/-}- and TRPV3^{-/-}-SG1 cells (*SI Appendix, Figs. S7B and S8 and Movie S7*). Furthermore, we expressed pHVenus-mCherry in the dorsal skin of TRPV3^{+/-} and TRPV3^{-/-} hairless mice via plasmid injection and subjected them to intravital pH_i imaging (*SI Appendix, Fig. S9*). This revealed that SG1 cells expressing pHVenus-mCherry displayed sustained mCherry signal but diminished pHVenus signal. These results suggested that the intracellular acidification of SG1 cells occurs normally in TRPV3^{-/-} mice. Therefore, these data suggest that the interval

between the $[Ca^{2+}]_i$ elevation and intracellular acidification (i.e., the duration time of phase I) is dysregulated in TRPV3^{-/-}-SG1 cells (Fig. 4H, SI Appendix, Figs. S7B and S8, and Movie S7).

Discussion

Possible Role of Phase I; $[Ca^{2+}]_i$ Elevation and Cell Membrane Permeabilization Triggered by High $[Ca^{2+}]_i$. Combining in vivo imaging and cell biological studies, we clarified the sequential events occurring during SG1 cell death (i.e., phase I (high $[Ca^{2+}]_i$ at neutral pH_i) and phase II (high $[Ca^{2+}]_i$ at acidic pH_i) (summarized in Fig. 5). Previous electron microscopic observation also described the existence of infrequently observed cells between SG and SC as “transitional cells” which possibly corresponded to the dying SG1 cells at late stage of phase II (30, 31).

What is the biological meaning of a prolonged high $[Ca^{2+}]_i$ (~60 min) under a “neutral pH_i” (phase I) versus short, spike-like $[Ca^{2+}]_i$ elevations that are generally observed in cultured cells? Intracellular Ca^{2+} overload is observed in other cell death types, including apoptosis, necrosis, autophagic cell death, pyroptosis, and NETosis (32–36). In SG1 cells, the prolonged increase in free cytosolic Ca^{2+} levels is assumed to either activate or induce conformational changes that influence various enzymes, such as caspases, calpains, other proteases, etc. Among these, TGases are Ca^{2+} -activated enzymes that catalyze protein covalent cross-linking events via the formation of isopeptide bonds (37). The CE is an insoluble protein structure of corneocytes replaced from plasma membranes. Elevated $[Ca^{2+}]_i$ in SG1 cells causes the activation of TGase 1 and TGase 3, which aid CE assembly underneath the plasma membrane, by cross-linking hydrophobic proteins, such as keratin 1/10, involucrin, loricrin, etc (13). Thus, maintaining high $[Ca^{2+}]_i$ in SG1 cells for a prolonged duration at a neutral pH, as seen in phase I, may be essential for achieving a complete cross-linking reaction at the site of CE formation.

Possible Roles of Phase II; Changes in Keratin and KHGs Triggered by Acidic pH_i. What is the biological meaning of rapid intracellular acidification under high $[Ca^{2+}]_i$ in SG1 cells? KHGs are

composed of keratin filament binding proteins with amorphous aggregated keratin filaments, such as profilaggrin (precursor of filaggrin), loricrin, and trichohyalin (18). Keratin intermediate filaments are supposedly affected by the intracellular acidification of SG1 cells (38–40). Furthermore, the disappearance of KHGs, which exist in a state of liquid–liquid phase separation, correlates with the drop in pH_i (below pH 6.2) of SG1 cells in vivo (41). This finding suggests that coincident with the rapid drop of pH_i in SG1 cells after ~60 min of “high $[Ca^{2+}]_i$ -neutral pH_i” (phase I), KHGs, and bundled keratin filaments change properties to become a component of stiff corneocytes.

For the disassembly of KHGs, profilaggrin-to-filaggrin processing is another key factor. Profilaggrin is composed of an N terminus, two Ca^{2+} -binding domains, tandemly connected filaggrin monomers (10 to 12 in human), and a C-terminus domain (18, 42, 43), and is localized at KHGs. During the SG1-to-SC transition, the linker sequences of profilaggrin are cleaved by specific proteases (44), such as SASPase, which is a retroviral-like aspartic (acid) protease with an optimum acidic pH for its activity (5.77 in mouse SASPase) (45, 46). One hypothesis raised by our results is that intracellular acidification may activate SASPase to accelerate profilaggrin processing. Cleaved filaggrin in corneocytes located in lower layers of the SC is involved in the bundling of keratin filaments (47).

Therefore, at the beginning of phase II (intracellular acidification of SG1 cells), the direct effect of an acidic pH as well as the bundling activity by the filaggrin monomer were suggested to enable the tight packing of keratin filaments well ahead of the formation of stiff corneocytes at the SG1-to-SC transition stage, at which point they begin to act as barriers in the SC (18).

Possible Roles of Phase II; Completion of DNA Degradation by Acidic pH_i. We demonstrated that isolated SG1 cells’ nuclear DNA was partially degraded in phase I and completely in phase II-mimicking conditions. The nuclei of SG1 cells are absent in the first layer of SC. Thus, nuclear degradation events must be

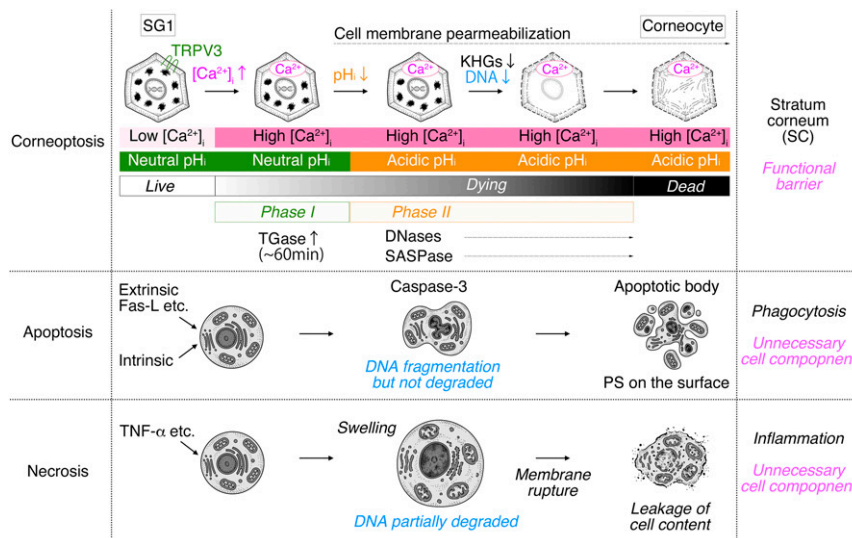


Fig. 5. A schematic illustration of the hypothetical cell death process of corneoptosis. In “corneoptosis,” corneocytes are formed after SG1 cell death through two sequential, intracellular states. “phase I:” high $[Ca^{2+}]_i$ -neutral pH_i activates TGases and lasts for ~60 min. “phase II:” high $[Ca^{2+}]_i$ -acidic pH_i induces the activation of DNases (DNase1L1 and DNase2), SASPase, and changes in the keratin network. As a result, KHGs are eliminated, the DNA is completely degraded, then the process of SG1 cell death is completed (black shaded bar), and corneocytes are formed. In apoptosis, extrinsic (Fas-L) or intrinsic factors activate the apoptotic pathway via the activation of effector caspases (such as caspase-3). Activated DNases fragment DNAs but do not degrade them completely. Organelles are degraded. Cytochrome C is released from the mitochondria. Chromatin is condensed. Cells finally form apoptotic bodies that present phosphatidylserine (PS) on their surface. PS is recognized by macrophages or adjacent cells that phagocytize dead cells and degrade all dead cell components. In necrosis, dead cells become swollen, and organelles/DNAs are partially degraded; subsequently, cell membranes are finally ruptured, and cell contents are leaked. This causes immune responses resulting in inflammation and the removal of cell remnants by immune cells via efferocytosis.

completed before/when the cells enter this layer. The major DNases expressed in differentiated epidermal layers are DNase1-like 2 (DNase1L2) and DNase2 (48, 49) and both have acidic optimal pH (50, 51). Moreover, the double inactivation of DNase1L2 and DNase2 in mouse skin showed a defect in the degradation of nuclear DNA in SG1 cells (52). It is reasonable to assume that nuclear acidification of SG1 cells is required for the full activation of these acid-activated DNases by phase II conditions for the completion of nuclear DNA degradation.

Corneoptosis as a Unique Cell Death Type Observed in SG1 Keratinocyte Cells. Taken together, our data suggest that SG1 cell death is complex and unique. We propose that several steps in the SG1 cell death process are essential to initiate cornification: 1) phase I—a long-lasting elevation in $[Ca^{2+}]_i$ at neutral pH_i for ~60 min, 2) phase II—a rapid drop in pH_i to achieve acidic conditions; and 3) elimination of KHGs and DNA and possibly other organelles, to form a mature corneocyte in the lower SC. Afterward, the corneocytes are retained in the SC, move upward, mature further, and eventually reach the SC surface and ultimately are shed (Fig. 5). In apoptosis or necrosis, dead cells are constantly removed by macrophages or nearby cells via efferocytosis. Otherwise, there is a leakage of cell content resulting in inflammation, as observed in necrosis (Fig. 5). The unique feature of SG1 cell death is that the dead cells (corneocytes) are not eliminated; rather, they function as an essential component of the SC barrier. Considering all the unique aspects of this cell death, we termed the SG1 cell death “corneoptosis,” the initial cornification process.

TRPV3 Acts as a Timekeeper for Phase I and Phase II during Corneoptosis in SG1 Cells. The observation of high temperature-evoked TRPV3-like currents in SG1 cells implied that the regulation of SG1 cell death by TRPV3 is differentially regulated at various body sites with different skin temperatures. Intravital $[Ca^{2+}]_i$ imaging of TRPV3-deficient mice revealed that increased $[Ca^{2+}]_i$ elevation frequencies were accompanied by the dysregulation of the timing of acidification in SG1 cells. This suggested that TRPV3 acts as a timekeeper for phase I and II conditions and also indicated that besides TRPV3, there might be another unidentified molecule(s) responsible for SG1-specific $[Ca^{2+}]_i$ elevation.

How does TRPV3 serve a timekeeper function? A unique feature of TRPV3 is its “sensitization mechanism;” the repeated stimulation of TRPV3 evokes, prolongs, and enhances multiple TRPV3 channel activities, possibly due to its structural characteristics (53–56). TRPV3^{-/-} mice exhibited aberrant epidermal

growth factor receptor signaling, resulting in abnormal hair morphogenesis and barrier formation-related defects (57). Moreover, a defect in the TGase activity was observed in the entire layer of the TRPV3-deficient epidermis. These mechanisms are attributable to the specific TRPV3-deficiency phenotype in SG1 cells, even though TRPV3 is expressed in all layers of the epidermis in humans and mice. A possible link between intracellular acidification and TRPV3 activation has been reported in case of nitric oxide production in cultured cells (58). Further studies are needed to understand the mechanism underlying the SG1-specific regulation of TRPV3.

Taken together, TRPV3 is suggested to play an important role in controlling the timing of acidification after $[Ca^{2+}]_i$ elevation in SG1 cells and maintaining the spatial and temporal homeostasis of corneoptosis in the epidermis.

Future Perspectives on the Study of Corneoptosis. Studying the corneoptosis process, which still requires the development of several new technologies, will allow us to understand the quality of the SC. The investigation of corneoptosis from the SG1 cell biological perspective will enable us to understand new aspects regarding cell death, which has a special biological meaning considering the mammalian skin.

Materials and Methods

Detailed experimental methods for intravital multiphoton excitation microscopy, confocal microscopy, isolation of SG1 cells, and whole-cell patch-clamp analysis of SG1 cells appear in *SI Appendix*.

Data Availability. Bam fastq data have been deposited in Gene Expression Omnibus (GSE168011).

ACKNOWLEDGMENTS. We thank Keiko Mizuno, Ritsuko Ozawa, Rika Yokoo, Sachie Marushima, Yuki Yamagishi, and Hachiro Iseki for technical assistance. We also thank Takashi Kondoh and Yusuke Iizuka, and Chieko Tezuka for generating TRPV3-deficient mice. We thank Dr. Takashi Hiiragi (European Molecular Biology Laboratory) and the Institute for Integrated Cell-Material Sciences, Kyoto University, for supporting this project. This study was supported by a Japan Agency for Medical Research and Development (AMED) under the Grant Numbers 19gm1010001, 18gm1010001, 19ek0410058, and 18ek0410028 by Health and Labour Sciences Research Grants for Research on Allergic Diseases and Immunology from the Ministry of Health, Labour and Welfare and by a Japan Society for the Promotion of Science (JSPS) Grant-in-Aid for Scientific Research (C) under the Grant Number JP25461667, by the Takeda Science Foundation, by the Naito Foundation, and by a Cooperative Study Program by the National Institute for Physiological Sciences, Japan. Y.F. was supported by a RIKEN Junior Research Associate Program. N.K. was supported by JSPS Grant-in-Aid for JSPS Fellows under Grant Number 19J00968. We thank Dr. Nick Parris for his critical reading of the manuscript.

1. J. F. Kerr, A. H. Wyllie, A. R. Currie, Apoptosis: A basic biological phenomenon with wide-ranging implications in tissue kinetics. *Br. J. Cancer* **26**, 239–257 (1972).
2. L. Galluzzi *et al.*, Molecular mechanisms of cell death: Recommendations of the nomenclature committee on cell death 2018. *Cell Death Differ.* **25**, 486–541 (2018).
3. G. Majno, I. Joris, Apoptosis, oncosis, and necrosis. An overview of cell death. *Am. J. Pathol.* **146**, 3–15 (1995).
4. S. Lippens, G. Denecker, P. Ovaere, P. Vandenaabee, W. Declercq, Death penalty for keratinocytes: Apoptosis versus cornification. *Cell Death Differ.* **12**, 1497–1508 (2005).
5. L. Eckhart, S. Lippens, E. Tschachler, W. Declercq, Cell death by cornification. *Biochim. Biophys. Acta* **1833**, 3471–3480 (2013).
6. T. Matsui, M. Amagai, Dissecting the formation, structure and barrier function of the stratum corneum. *Int. Immunol.* **27**, 269–280 (2015).
7. L. Alibardi, Adaptation to the land: The skin of reptiles in comparison to that of amphibians and endotherm amniotes. *J. Exp. Zool. B Mol. Dev. Evol.* **298**, 12–41 (2003).
8. F. M. Watt, Terminal differentiation of epidermal keratinocytes. *Curr. Opin. Cell Biol.* **1**, 1107–1115 (1989).
9. M. Yokouchi *et al.*, Epidermal cell turnover across tight junctions based on Kelvin's tetraikadecahedron cell shape. *eLife* **5**, e19593 (2016).
10. K. Hashimoto, Intercellular spaces of the human epidermis as demonstrated with lanthanum. *J. Invest. Dermatol.* **57**, 17–31 (1971).
11. M. Furuse *et al.*, Claudin-based tight junctions are crucial for the mammalian epidermal barrier: A lesson from claudin-1-deficient mice. *J. Cell Biol.* **156**, 1099–1111 (2002).
12. D. Tsuruta, K. J. Green, S. Getsios, J. C. Jones, The barrier function of skin: How to keep a tight lid on water loss. *Trends Cell Biol.* **12**, 355–357 (2002).
13. E. Candi, R. Schmidt, G. Melino, The cornified envelope: A model of cell death in the skin. *Nat. Rev. Mol. Cell Biol.* **6**, 328–340 (2005).
14. S. Ipponjima, Y. Umino, M. Nagayama, M. Denda, Live imaging of alterations in cellular morphology and organelles during cornification using an epidermal equivalent model. *Sci. Rep.* **10**, 5515 (2020).
15. C. L. Simpson *et al.*, NIX initiates mitochondrial fragmentation via DRP1 to drive epidermal differentiation. *Cell Rep.* **34**, 108689 (2021).
16. C. R. Harding *et al.*, The cornified cell envelope: An important marker of stratum corneum maturation in healthy and dry skin. *Int. J. Cosmet. Sci.* **25**, 157–167 (2003).
17. T. Richter *et al.*, Dead but highly dynamic—The stratum corneum is divided into three hydration zones. *Skin Pharmacol. Physiol.* **17**, 246–257 (2004).
18. A. Sandilands, C. Sutherland, A. D. Irvine, W. H. McLean, Filaggrin in the frontline: Role in skin barrier function and disease. *J. Cell Sci.* **122**, 1285–1294 (2009).
19. A. Kubo *et al.*, The stratum corneum comprises three layers with distinct metal-ion barrier properties. *Sci. Rep.* **3**, 1731 (2013).
20. P. M. Elias *et al.*, The secretory granular cell: The outermost granular cell as a specialized secretory cell. *J. Investig. Dermatol. Symp. Proc.* **3**, 87–100 (1998).
21. K. A. Holbrook, Biologic structure and function: Perspectives on morphologic approaches to the study of the granular layer keratinocyte. *J. Invest. Dermatol.* **92**, 845–1045 (1989).
22. T. Murata *et al.*, Transient elevation of cytoplasmic calcium ion concentration at a single cell level precedes morphological changes of epidermal keratinocytes during cornification. *Sci. Rep.* **8**, 6610 (2018).

23. S. H. Bokman, W. W. Ward, Renaturation of Aequorea gree-fluorescent protein. *Biophys. Res. Commun.* **101**, 1372–1380 (1981).
24. Y. Zhao *et al.*, An expanded palette of genetically encoded Ca²⁺ indicators. *Science* **333**, 1888–1891 (2011).
25. M. Ohkura, T. Sasaki, C. Kobayashi, Y. Ikegaya, J. Nakai, An improved genetically encoded red fluorescent Ca²⁺ indicator for detecting optically evoked action potentials. *PLoS One* **7**, e39933 (2012).
26. T. Tojima *et al.*, Attractive axon guidance involves asymmetric membrane transport and exocytosis in the growth cone. *Nat. Neurosci.* **10**, 58–66 (2007).
27. M. Amagai, N. Matsuyoshi, Z. H. Wang, C. Andl, J. R. Stanley, Toxin in bullous impetigo and staphylococcal scalded-skin syndrome targets desmoglein 1. *Nat. Med.* **6**, 1275–1277 (2000).
28. A. M. Peier *et al.*, A heat-sensitive TRP channel expressed in keratinocytes. *Science* **296**, 2046–2049 (2002).
29. H. Xu *et al.*, TRPV3 is a calcium-permeable temperature-sensitive cation channel. *Nature* **418**, 181–186 (2002).
30. I. Brody, An ultrastructural study on the role of the keratohyalin granules in the keratinization process. *J. Ultrastruct. Res.* **3**, 84–104 (1959).
31. I. Brody, The ultrastructure of the tonofibrils in the keratinization process of normal human epidermis. *J. Ultrastruct. Res.* **4**, 264–297 (1960).
32. S. Orrenius, B. Zhivotovsky, P. Nicotera, Regulation of cell death: The calcium-apoptosis link. *Nat. Rev. Mol. Cell Biol.* **4**, 552–565 (2003).
33. M. W. Harr, C. W. Distelhorst, Apoptosis and autophagy: Decoding calcium signals that mediate life or death. *Cold Spring Harb. Perspect. Biol.* **2**, a005579 (2010).
34. B. Zhivotovsky, S. Orrenius, Calcium and cell death mechanisms: A perspective from the cell death community. *Cell Calcium* **50**, 211–221 (2011).
35. A. K. Gupta, S. Giaglis, P. Hasler, S. Hahn, Efficient neutrophil extracellular trap induction requires mobilization of both intracellular and extracellular calcium pools and is modulated by cyclosporine A. *PLoS One* **9**, e97088 (2014).
36. N. M. de Vasconcelos, N. Van Opdenbosch, H. Van Gorp, E. Parthoens, M. Lamkanfi, Single-cell analysis of pyroptosis dynamics reveals conserved GSDMD-mediated sub-cellular events that precede plasma membrane rupture. *Cell Death Differ.* **26**, 146–161 (2019).
37. L. Lorand, R. M. Graham, Transglutaminases: Crosslinking enzymes with pleiotropic functions. *Nat. Rev. Mol. Cell Biol.* **4**, 140–156 (2003).
38. C. H. Lee, P. A. Coulombe, Self-organization of keratin intermediate filaments into cross-linked networks. *J. Cell Biol.* **186**, 409–421 (2009).
39. L. Ma, S. Yamada, D. Wirtz, P. A. Coulombe, A 'hot-spot' mutation alters the mechanical properties of keratin filament networks. *Nat. Cell Biol.* **3**, 503–506 (2001).
40. S. Yamada, D. Wirtz, P. A. Coulombe, Pairwise assembly determines the intrinsic potential for self-organization and mechanical properties of keratin filaments. *Mol. Biol. Cell* **13**, 382–391 (2002).
41. F. G. Quiroz *et al.*, Liquid-liquid phase separation drives skin barrier formation. *Science* **367**, eaax9554 (2020).
42. R. B. Presland, J. A. Bassuk, J. R. Kimball, B. A. Dale, Characterization of two distinct calcium-binding sites in the amino-terminus of human profilaggrin. *J. Invest. Dermatol.* **104**, 218–223 (1995).
43. S. J. Brown, W. H. McLean, One remarkable molecule: Filaggrin. *J. Invest. Dermatol.* **132**, 751–762 (2012).
44. S. J. de Veer, L. Furio, J. M. Harris, A. Hovnanian, Proteases: Common culprits in human skin disorders. *Trends Mol. Med.* **20**, 166–178 (2014).
45. T. Matsui *et al.*, Mouse homologue of skin-specific retroviral-like aspartic protease involved in wrinkle formation. *J. Biol. Chem.* **281**, 27512–27525 (2006).
46. T. Matsui *et al.*, SASPase regulates stratum corneum hydration through profilaggrin-to-filaggrin processing. *EMBO Mol. Med.* **3**, 320–333 (2011).
47. B. A. Dale, K. A. Holbrook, P. M. Steinert, Assembly of stratum corneum basic protein and keratin filaments in macrofibrils. *Nature* **276**, 729–731 (1978).
48. H. Fischer *et al.*, DNase1L2 degrades nuclear DNA during corneocyte formation. *J. Invest. Dermatol.* **127**, 24–30 (2007).
49. H. Fischer *et al.*, DNase 2 is the main DNA-degrading enzyme of the stratum corneum. *PLoS One* **6**, e17581 (2011).
50. D. Shiokawa, S. Tanuma, Characterizing of human DNase I family endonucleases and activation of DNase gamma during apoptosis. *Biochemistry* **40**, 143–152 (2001).
51. L. Eckhart, H. Fischer, K. B. Barken, T. Tolker-Nielsen, E. Tschachler, DNase1L2 suppresses biofilm formation by *Pseudomonas aeruginosa* and *Staphylococcus aureus*. *Br. J. Dermatol.* **156**, 1342–1345 (2007).
52. H. Fischer, M. Buchberger, M. Napirei, E. Tschachler, L. Eckhart, Inactivation of DNase1L2 and DNase2 in keratinocytes suppresses DNA degradation during epidermal cornification and results in constitutive parakeratosis. *Sci. Rep.* **7**, 6433 (2017).
53. A. Moqrich *et al.*, Impaired thermosensation in mice lacking TRPV3, a heat and camphor sensor in the skin. *Science* **307**, 1468–1472 (2005).
54. A. K. Singh *et al.*, Structural basis of temperature sensation by the TRP channel TRPV3. *Nat. Struct. Mol. Biol.* **26**, 994–998 (2019).
55. Z. Deng *et al.*, Gating of human TRPV3 in a lipid bilayer. *Nat. Struct. Mol. Biol.* **27**, 635–644 (2020).
56. H. Shimada *et al.*, The structure of lipid nanodisc-reconstituted TRPV3 reveals the gating mechanism. *Nat. Struct. Mol. Biol.* **27**, 645–652 (2020).
57. X. Cheng *et al.*, TRP channel regulates EGFR signaling in hair morphogenesis and skin barrier formation. *Cell* **141**, 331–343 (2010).
58. T. Miyamoto, M. J. Petrus, A. E. Dubin, A. Patapoutian, TRPV3 regulates nitric oxide synthase-independent nitric oxide synthesis in the skin. *Nat. Commun.* **2**, 369 (2011).